Int J Adv Manuf Technol (2015) 79:1453–1463
DOI 10.1007/s00170-015-6929-1

ORIGINAL ARTICLE

Position-dependent stability analysis of turning with tool and workpiece compliance

Andreas Otto · Firas A. Khasawneh · Günter Radons

Received: 7 October 2014 / Accepted: 20 February 2015 / Published online: 5 March 2015

Abstract A universal frequency domain approach for studying the dynamics of metal cutting with a flexible workpiece and a compliant tool is derived. The method is used for the identification of the position-dependent stability lobes in turning. It enables a fast, accurate, and systematic stability analysis of turning processes in the parameter space, which is not restricted to simple dynamic models with only a specific number of modes in one spatial direction. In particular, a combination of experimental data for the tool tip dynamics with analytical or numerical data for the workpiece dynamics is possible, which is demonstrated by a concrete example. The effect of the mode interaction between tool and workpiece modes via the cutting process is illustrated. Counterintuitively, the possibility of a process destabilization for an increased workpiece stiffness was observed, which can be explained by the mode interaction. The presented methods and results can be efficiently used for optimizing machine tool development and process planning.

Keywords Chatter · Vibration · Stability · Turning · Boring · Beam theory

A. Otto (✉) · G. Radons
Institute of Physics, Chemnitz University of Technology, 09107 Chemnitz, Germany
e-mail: andreas.otto@physik.tu-chemnitz.de

F. A. Khasawneh
Mechanical Engineering, SUNY Polytechnic Institute, Utica, NY 13502, USA

1 Introduction

Machine tool chatter has been a rich topic of research for over 50 years. The interest in chatter phenomena is driven by the manufacturing industry's desire for maximizing metal removal rates while maintaining acceptable surface finish and tool life. As the machining technology advances and needs for new products emerge, chatter continues to be one of the main impediments to high productivity. One example of modern manufacturing processes where chatter plays an important role is machining of slender components for aerospace, medical, and energy industries.

There have been many studies on machining dynamics where the tool is assumed to be compliant while the workpiece is assumed to be rigid [1–4]. However, the number of studies on machining slender structures is significantly smaller due to modeling and computational challenges associated with machining flexible structures. Some of these challenges include the variation in the workpiece characteristics due to metal removal and tool position, and the increased number of degrees of freedom due to the flexibility of both the tool and the workpiece. Flexible structures are often modeled using partial differential equations with possibly several modes contributing to the onset of chatter. The situation is further complicated because in general the tool is also compliant and the motions of the tool and the workpiece are coupled by the cutting process at the tool tip.

A large number of studies on machining flexible workpieces solely focus on the workpiece dynamics. Several of these studies use computationally expensive numerical simulations and finite element modeling to obtain accurate workpiece dynamics while the interaction between the workpiece and the tool dynamics is not taken into account [5–7].

Semi-analytical methods based on time domain analysis have also been used to investigate machining of compliant structures. For example, Song et al. used semi-discretization for studying the stability in milling a thin workpiece [8] while Urbikain et al. used a Chebyshev collocation method for the stability analysis of turning a flexible workpiece [9]. In both studies, only the dynamics in one spatial direction and only one dominant mode is considered. Eksioglu et al. simulated and studied the stability in milling a flexible workpiece using semi-discretization [10]. Both the tool and the workpiece were assumed to be flexible along one spatial direction. Time domain methods can be useful especially for systems with time-varying coefficients; however, they are not ideal if a large number of modes are needed in the analysis.

The above limitations of time domain simulations have made frequency domain methods more attractive for studying machining of flexible structures. Thevenot et al. studied the stability of a single degree of freedom end milling process [11]. The tool was assumed to be rigid while the workpiece was assumed to be flexible. Bravo et al. studied milling of monolithic components with flexible tools [12]. They showed that the interaction between tool and workpiece dynamics is important for a reliable prediction of the process dynamics. In [12] different geometries of the workpiece corresponding to different machining stages were taken into account but no position-dependent dynamics was calculated. The authors of [13–16] studied the stability in turning with and without tailstock-supported workpiece. However, their methods are restricted to a specific number of modes along one spatial direction.

In this paper, a generic frequency domain method for the quick and reliable identification of the stability lobes in turning is derived. This method takes into account the flexibility of both the workpiece and the tool. In contrast to the existing literature, the position-dependent stability analysis for an arbitrary number of modes in any spatial direction is presented. Moreover, the combination of experimental and numerical data for the tool and workpiece dynamics is shown. Therefore, the present approach makes the full power of frequency domain methods available for the position-dependent stability analysis in metal cutting. Specifically, the present approach enables fast computations and parameter studies with complex models or experimental results as input data. Position-dependent stability lobes are calculated for a simple model from the literature and a complex model based on experimental data. The oriented transfer function [17] is used to study the influence of varying the cutting point, lead angle, and boundary conditions on the critical depth of cut via Tlusty's law. The effects of the mode coupling between tool and workpiece modes via the cutting process is illustrated. The results show the possibility of process stabilization through decreasing the workpiece stiffness.

2 Dynamic cutting model

The dynamic cutting model consists of a model for the machine tool dynamics at the tool tip, a modal description for the workpiece dynamics at the cutting point, and a cutting force model.

2.1 Tool tip dynamics

The geometry of the turning process is illustrated in Fig. 1a. The dynamic displacement of the tool tip $\mathbf{r}_t(t) = (x_t(t), y_t(t), z_t(t))^T$ in Cartesian coordinates is expanded in a superposition of modal displacements of the first N_t tool modes

$$\mathbf{r}_t(t) = \mathbf{V}_t \mathbf{q}_t(t). \tag{1}$$

The vector $\mathbf{q}_t(t)$ contains the modal displacements $q_{t,j}(t)$, $j = 1, \ldots, N_t$ and the columns of the $3 \times N_t$ dimensional matrix $\mathbf{V}_t$ are the mode shapes $\mathbf{v}_{t,j}$ of the tool modes in Cartesian coordinates evaluated at the tool tip. The dynamics of the tool modes can be described by the equation of motion

$$\mathbf{M}_t \ddot{\mathbf{q}}_t(t) + \mathbf{C}_t \dot{\mathbf{q}}_t(t) + \mathbf{K}_t \mathbf{q}_t(t) = \mathbf{V}_t^T \mathbf{F}(P, t), \tag{2}$$

where ^{T} denotes transposition. The matrices $\mathbf{M}_t$, $\mathbf{C}_t$, and $\mathbf{K}_t$ are the modal mass, damping, and stiffness matrices for the dynamics at the tool tip and the vector $\mathbf{F}(P, t) = \big(F_x(P, t), F_y(P, t), F_z(P, t)\big)^T$ contains the cutting force components in Cartesian coordinates acting on the tool tip at the cutting point P. The entries of the matrices $\mathbf{M}_t$, $\mathbf{C}_t$, $\mathbf{K}_t$, and $\mathbf{V}_t$ can be determined by using an analytical or finite element model for the machine tool structure. Alternatively, in Section 3, we show the implementation of experimentally measured frequency response functions (FRFs) for the tool tip dynamics.

2.2 Workpiece dynamics

The workpiece is assumed to be rigid in the z-direction. In addition, vibrations in the y-direction are not considered because the influence of tangential vibrations on the limiting chip width in turning is typically very low [18]. Euler-Bernoulli beam theory similar to [13] is used to describe the workpiece displacements in x-direction. The moment produced by the cutting force in the z-direction and the variation of the workpiece diameter D due to cutting are neglected. The extension to a more accurate model as in [7]

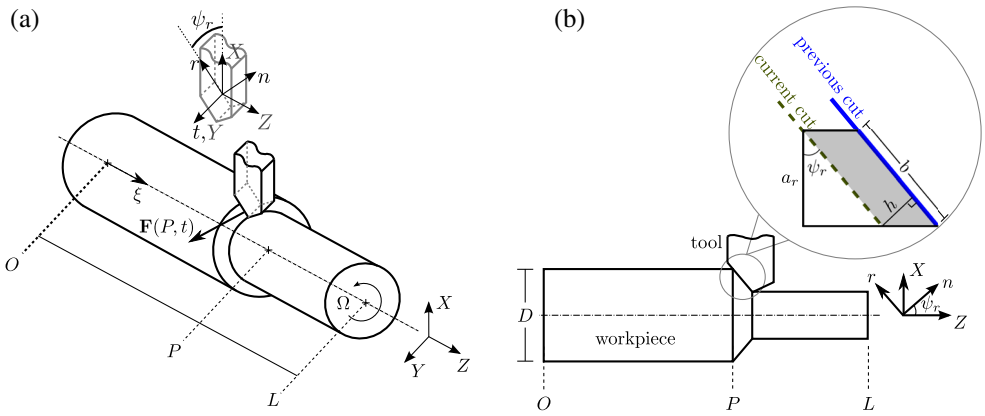

Fig. 1 **a** Model for turning of a cylindrical workpiece of length L and diameter D at cutting point P with cutting force $\mathbf{F}(P,t)$ acting on the tool tip. **b** The uncut chip area (shaded parallelogram) is the product of the chip thickness h and the chip width b. The chip thickness depends on the relative displacement between the cutting edge and the workpiece along the normal direction n at the current (*green*, *dashed*) and the previous (*blue, thick*) cuts (cf. 13)

or to Timoshenko beam theory as in [5] is straightforward but is not shown in this paper.

The equation of motion for the x-displacement of the workpiece $x_w(\xi,t)$ dependent on the reference axial coordinate ξ and time t is

$$\rho A\frac{\partial^2 x_w(\xi,t)}{\partial t^2}+EI\frac{\partial^4 x_w(\xi,t)}{\partial \xi^4}=-F_x(\xi,t)\delta(\xi-P). \quad (3)$$

Here, ρ is the density, $A=\pi D^2/4$ is the cross-sectional area, E is the modulus of elasticity, and I is the area moment of inertia of the workpiece. The cutting force $F_x(\xi,t)$ in the x-direction is approximated via a point load at the cutting point P and the negative sign is due to Newtons action-reaction law. Similar to Eq. 1 for the tool dynamics, the workpiece displacement $\mathbf{r}_w(\xi,t)=(x_w(\xi,t),0,0)^T$ can be expressed via a superposition of the first N_w workpiece modes

$$\mathbf{r}_w(\xi,t)=\mathbf{V}_w(\xi)\mathbf{q}_w(t). \quad (4)$$

In contrast to Eq. 1, in Eq. 4, the $3\times N_w$ dimensional matrix $\mathbf{V}_w(\xi)$ of the workpiece mode shapes $\mathbf{v}_{w,j}(\xi)$ depends on the reference axial position ξ with the second and third row corresponding to the y and z components set to zero. The workpiece eigenmodes are mutually orthonormal according to

$$\frac{1}{L}\int_0^L \mathbf{V}_w^T(\xi)\mathbf{V}_w(\xi)d\xi=\mathbf{I}, \quad (5)$$

where $\mathbf{I}$ is the $N_w\times N_w$ identity matrix. Combining (3) and (4), multiplying by $\mathbf{V}_w^T(\xi)$ from the left, integrating over the length L of the beam and using Eq. 5 results in

$$\mathbf{M}_w\ddot{\mathbf{q}}_w(t)+\mathbf{K}_w\mathbf{q}_w(t)=-\mathbf{V}_w^T(P)\mathbf{F}(P,t). \quad (6)$$

In Eq. 6, $\mathbf{M}_w=\rho AL\mathbf{I}$ and $\mathbf{K}_w$ are $N_w\times N_w$ diagonal matrices with the workpiece mass $m_w=\rho AL$ and, respectively, the modal stiffnesses $m_w\omega_{w,j}$ on their main diagonals.

The mode shapes $\mathbf{v}_{w,j}(\xi)$ and the eigenfrequencies $\omega_{w,j}$ of the workpiece modes are determined by the eigenvectors and, respectively, the eigenvalues of the boundary value problem

$$LEI\mathbf{v}''''_{w,j}(\xi)-m_w\omega^2_{w,j}\mathbf{v}_{w,j}(\xi)=0. \quad (7)$$

In this paper, the left end of the workpiece is fixed to the chuck ($\mathbf{v}_{w,j}(0)=0$, $\mathbf{v}'_{w,j}(0)=0$) while the right end is either free ($\mathbf{v}''_{w,j}(L)=0$, $\mathbf{v}'''_{w,j}(L)=0$) or pinned ($\mathbf{v}_{w,j}(L)=0$, $\mathbf{v}''_{w,j}(L)=0$). The fixed-free and the fixed-pinned boundary conditions are used to approximate turning a cantilevered or tailstock-supported workpiece, respectively. The ideal fixed-pinned boundary conditions are also used in [7], and verified experimentally. Non-ideal boundary conditions can be taken into account by permitting small deflections in the boundary conditions [19].

The stability lobes are sensitive to damping because the limiting chip width is proportional to the damping ratio of the structure [20]. Without damping, the minimum limiting chip width becomes zero which obviously does not represent the real cutting dynamics. Therefore, in contrast to [13], workpiece damping is introduced in Eq. 6 to account for energy dissipation. Workpiece damping is typically low; thus, it is assumed that the workpiece eigenmodes, i.e., the matrix $\mathbf{V}_w(\xi)$, does not change with the introduction of damping. For example, this can be realized by introducing proportional (Rayleigh) damping or generalized proportional damping in the equation of motion [21]. With the addition of damping, the equation of motion for the workpiece in modal coordinates reads

$$\mathbf{M}_w\ddot{\mathbf{q}}_w(t)+\mathbf{C}_w\dot{\mathbf{q}}_w(t)+\mathbf{K}_w\mathbf{q}_w(t)=-\mathbf{V}_w^T(P)\mathbf{F}(P,t). \quad (8)$$

In Eq. 8, the matrices $\mathbf{M}_w$, $\mathbf{K}_w$, and $\mathbf{V}_w(\xi)$ can be obtained from an FE model or an analytical model, e.g., the presented Euler-Bernoulli beam model. The parameters of the diagonal modal damping matrix $\mathbf{C}_w$ can be determined by measuring FRFs of the workpiece dynamics [21]. In contrast to the direct implementation of the FRF measurements,

the presented workpiece model permits the specification of the workpiece dynamics for different cutting points $\xi = P$ due to the known workpiece mode shapes $\mathbf{V}_w(\xi)$.

2.3 Combined model

Equations 2 and 8 for the dynamics of the tool and the workpiece can be combined. The displacements of the tool and the workpiece generate the relative dynamic displacements $\mathbf{r}(\xi,t) = \mathbf{r}_t(t) - \mathbf{r}_w(\xi,t)$ in Cartesian coordinates. These relative displacements can be written as a modal expansion according to

$$\mathbf{r}(\xi,t) = \mathbf{V}(\xi)\mathbf{q}(t). \tag{9}$$

The definition $\mathbf{q}^T(t) = \left(\mathbf{q}_t^T(t), -\mathbf{q}_w^T(t)\right)$ for the $N = N_t + N_w$ dimensional vector, containing the modal displacements $q_j(t)$, accounts for the opposite sign in the contribution of tool $\mathbf{r}_t(t)$ and workpiece displacements $\mathbf{r}_w(\xi,t)$ to the relative displacements $\mathbf{r}(\xi,t)$. The $3 \times N$ dimensional matrix $\mathbf{V}(\xi)$ for the mode shapes of the combined model is defined by $\mathbf{V}(\xi) = [\mathbf{V}_t, \mathbf{V}_w(\xi)]$. The dynamics of the combined structure with tool and workpiece modes can be described by the N-dimensional differential equation

$$\mathbf{M}\ddot{\mathbf{q}}(t) + \mathbf{C}\dot{\mathbf{q}}(t) + \mathbf{K}\mathbf{q}(t) = \mathbf{V}^T(P)\mathbf{F}(P,t), \tag{10}$$

where the modal mass, damping, and stiffness matrices $\mathbf{M}$, $\mathbf{C}$, and $\mathbf{K}$ are diagonal matrices with the corresponding masses m_j, damping $m_j 2\zeta_j\omega_j$ and stiffness values $m_j\omega_j^2$, $j = 1,\ldots N$ of the tool and workpiece modes on the main diagonal.

2.4 Cutting force

According to Fig. 1, the cutting force vector $\mathbf{F}(P,t)$ at time t and cutting point P in Cartesian coordinates, representing the force on the tool, can be obtained from the cutting force vector $\mathbf{F}_e(P,t) = (F_t(P,t), F_n(P,t), F_r(P,t))$ in cutting edge coordinates by the coordinate transformation

$$\begin{aligned}\mathbf{F}(P,t) &= \mathbf{T}\mathbf{F}_e(P,t)\\ &= \begin{pmatrix} 0 & \sin\psi_r & \cos\psi_r \\ 1 & 0 & 0 \\ 0 & \cos\psi_r & -\sin\psi_r \end{pmatrix} \begin{pmatrix} F_t(P,t) \\ F_n(P,t) \\ F_r(P,t) \end{pmatrix},\end{aligned} \tag{11}$$

with the lead angle ψ_r. The cutting force in cutting edge coordinates $\mathbf{F}_e(P,t)$ is divided into a tangential component $F_t(P,t)$ parallel to the cutting velocity in y-direction, a normal component $F_n(P,t)$ perpendicular to a plane formed by the cutting velocity and the cutting edge and a radial component $F_r(P,t)$ parallel to the cutting edge similar to [22]. Details on the specification of the tangential cutting pressure K_t, and the ratios between normal and radial versus tangential cutting pressure, k_n and k_r, respectively, can be found in [17] and references therein. The force in edge coordinates can be determined from

$$\mathbf{F}_e(P,t) = bK_t \begin{pmatrix} 1 \\ k_n \\ k_r \end{pmatrix} h(P,t), \tag{12}$$

where b is the chip width and $h(P,t)$ is the chip thickness at time t and cutting point P. Note that the chip thickness $h(P,t)$ and the chip width b, respectively, are measured in normal and radial direction of the edge coordinates (cf. Fig. 1b). For comparing cylindrical turning processes with different lead angles, the depth of cut $a_r = b\cos\psi_r$, i.e., the width of the cut in x-direction, is defined according to Fig. 1b. In Eq. 12, the influence of process damping is neglected, but its inclusion is straightforward as described in [23].

The chip thickness $h(P,t)$ is composed of a static part h_0 due to the feed per revolution and a dynamic part due to the oscillations of the tool and the workpiece. For grooving operations ($\psi_r = 90°$), the feed motion is in the negative x-direction, and for cylindrical turning ($\psi_r < 90°$), the feed motion is in the negative z-direction. It is assumed that the dynamic part is always smaller than the static part h_0, i.e., the tool does not lose contact with the workpiece. The static part h_0 of the chip thickness $h(P,t)$ has no influence on the process stability and is therefore dropped from the analysis. The dynamic part of the chip thickness is defined by the projection of the relative dynamic displacements from two consecutive revolutions onto the normal direction. Figure 1b shows the relative dynamic displacements at the current $\mathbf{r}(P,t)$ and the previous $\mathbf{r}(P,t-\tau)$ cuts with dashed (green) and thick (blue) lines, respectively. The corresponding expression for the dynamic chip thickness reads

$$\begin{aligned} h(P,t) &= (\sin\psi_r, 0, \cos\psi_r)\left(\mathbf{r}(P,t-\tau) - \mathbf{r}(P,t)\right)\\ &= \mathbf{e}_n^T\left(\mathbf{r}(P,t-\tau) - \mathbf{r}(P,t)\right). \end{aligned} \tag{13}$$

In Eq. 13, the vector $\mathbf{e}_n$ defines the direction of the normal component of the cutting force, i.e., $\mathbf{e}_n$ is equal to the second column of the matrix $\mathbf{T}$ in Eq. 11. The time delay τ is equal to the period of one spindle revolution. Since the cutting points for the present and the previous cuts are assumed to be constant and equal to P, Eq. 13 represents a quasistatic approximation of the chip thickness and the process dynamics. This approximation is valid as long as the feed per revolution is much smaller than the length of the workpiece.

Combining (11), (12), and (13), the cutting force can be written as

$$\mathbf{F}(P,t) = bK_t\mathbf{B}_r\left(\mathbf{r}(P,t-\tau) - \mathbf{r}(P,t)\right). \tag{14}$$

The 3×3 dimensional coefficient matrix $\mathbf{B}_r$ of the so-called directional factors in Cartesian coordinates is defined by

$$\mathbf{B}_r = \mathbf{T} \begin{pmatrix} 1 \\ k_n \\ k_r \end{pmatrix} \mathbf{e}_n^T, \tag{15}$$

which is similar to the definition in [23].

3 Position-dependent stability analysis

In this section, the position-dependent stability analysis is described for varying cutting points P. Since the coefficients of the equation of motion (10) and the coefficients of the cutting force vector in Eq. 14 are constant, the analysis in the frequency domain is suitable. The stability lobes specify the limiting chip width b_{lim} for a given spindle speed $\Omega = 2\pi/\tau$. For chip widths $b > b_{\text{lim}}$, the process is unstable and the amplitude of chatter vibrations increases, whereas for $b < b_{\text{lim}}$ the amplitude of vibrations due to perturbations decreases. Thus, a purely periodic relative motion of the structure with chatter frequency ω_c and constant amplitude can be considered for the calculation of the stability lobes. The Fourier transformation

$$\hat{\mathbf{u}}(\omega) = \frac{1}{\sqrt{2\pi}} \int_{-\infty}^{\infty} \mathbf{u}(t)\, \mathbf{e}^{-i\omega t} dt \tag{16}$$

is used to transform some vector $\mathbf{u}(t)$ from the time domain to the frequency domain.

3.1 Closed loop representation of chatter in different coordinates

With the aid of Eq. 16, the frequency domain representation of Eq. 10 is found for the description of the structural dynamics

$$\hat{\mathbf{q}}(\omega) = \Phi_q(\omega)\mathbf{V}^T(P)\hat{\mathbf{F}}(P, \omega), \tag{17}$$

where $\Phi_q(\omega)$ is the $N \times N$ dimensional diagonal matrix, containing the modal FRFs $\Phi_{q,j}(\omega)$ on the main diagonal,

$$\Phi_{q,j}(\omega) = \frac{1}{m_j \left(\omega_j^2 - \omega^2 + 2\zeta_j \omega_j i\omega\right)}. \tag{18}$$

Equation (14) for the cutting force can be written in the frequency domain by

$$\hat{\mathbf{F}}(P, \omega) = bK_t \left(\mathbf{e}^{-i\omega\tau} - 1\right) \mathbf{B}_r \hat{\mathbf{r}}(P, \omega). \tag{19}$$

Substituting Eq. 19 into Eq. 17 and using the frequency domain representation of the modal expansion (9) for the relative displacements $\hat{\mathbf{r}}(P, \omega)$ yields the closed loop representation of regenerative chatter in modal coordinates

$$\hat{\mathbf{q}}(\omega) = bK_t \left(\mathbf{e}^{-i\omega\tau} - 1\right) \Phi_q(\omega)\mathbf{B}_q(P)\hat{\mathbf{q}}(\omega). \tag{20}$$

Here, $\mathbf{B}_q(P) = \mathbf{V}^T(P)\mathbf{B}_r\mathbf{V}(P)$ is the $N \times N$ dimensional matrix of the directional factors in modal coordinates depending on the cutting point P.

Multiplying (20) with $\mathbf{V}(P)$ from the left results in the representation of the closed loop for regenerative chatter in Cartesian coordinates

$$\hat{\mathbf{r}}(P, \omega) = bK_t \left(\mathbf{e}^{-i\omega\tau} - 1\right) \Phi_r(P, \omega)\mathbf{B}_r \hat{\mathbf{r}}(P, \omega). \tag{21}$$

In contrast to the modal FRF matrix $\Phi_q(\omega)$, the matrix $\Phi_r(P, \omega) = \mathbf{V}(P)\Phi_q(\omega)\mathbf{V}^T(P)$ specifies the structural dynamic behavior in Cartesian coordinates, which depends on the cutting point P. The entries $\{\Phi_r(P, \omega)\}_{ij}$, $i, j \in \{x, y, z\}$, describe the displacements along i in response to a force acting along j on the structure at cutting point P with frequency ω.

Another variable transformation $\hat{h}(P, \omega) = \mathbf{e}_n^T \hat{\mathbf{r}}(P, \omega)$ converts (21) to a scalar relationship describing the vibrations in the normal direction $\mathbf{e}_n$

$$\hat{h}(P, \omega) = bK_t \left(\mathbf{e}^{-i\omega\tau} - 1\right) \sigma(P, \omega)\hat{h}(P, \omega). \tag{22}$$

Equation (22) is the closed loop representation of regenerative chatter for chip thickness variations. The corresponding oriented transfer function $\sigma(P, \omega) = \sigma_{\text{R}}(P, \omega) + i\sigma_{\text{I}}(P, \omega)$ for the turning process is defined by

$$\sigma(P, \omega) = \mathbf{e}_n^T \Phi_r(P, \omega)\mathbf{T} \begin{pmatrix} 1 \\ k_n \\ k_r \end{pmatrix}. \tag{23}$$

Equation (22) shows that the regenerative effect in turning is a one-dimensional problem because only vibrations in the fixed normal direction $\mathbf{e}_n$ affect the chip thickness $h(P, t)$ and the cutting force $\mathbf{F}(P, t)$. In fact, consistent with [23], the oriented transfer function $\sigma(P, \omega)$ is the only nonzero eigenvalue of the matrix products $\Phi_q(\omega)\mathbf{B}_q(P)$ and $\Phi_r(P, \omega)\mathbf{B}_r$ corresponding to Eqs. 20 and 21, respectively.

3.2 Identification of stability lobes

Following the argumentation in [23], the limiting chip width b_{lim} can be calculated using the eigenvalue

$$\lambda(P, \omega, \tau) = \lambda_{\text{R}}(P, \omega, \tau) + i\lambda_{\text{I}}(P, \omega, \tau) = \left(\mathbf{e}^{-i\omega\tau} - 1\right) \sigma(P, \omega). \tag{24}$$

Due to a real-valued chip width b and tangential cutting pressure K_t, Eq. 22 can only be fulfilled if the imaginary part of this eigenvalue vanishes

$$\lambda_{\text{I}}(P, \omega, \tau) = 0. \tag{25}$$

Consequently, the associated chip widths are defined by

$$b(P,\omega,\tau)=\frac{1}{K_t\lambda_{\mathrm{R}}(P,\omega,\tau)}. \tag{26}$$

For a fixed cutting point P and delay τ, Eqs. 25 and 26 specify infinitely many pairs of frequencies $\omega = \omega_{\mathrm{cr}}$ and critical chip widths $b_{\mathrm{cr}} = b(P,\omega_{\mathrm{cr}},\tau)$ where purely periodic vibrations of the structure are possible. However, only the minimum value $b_{\mathrm{lim}} = \min b_{\mathrm{cr}}$ of the critical chip widths defines the stability boundary that separates stable and unstable regions. The chatter frequency ω_c is the critical frequency which corresponds to the limiting chip width, $b_{\mathrm{lim}} = b(P,\omega_c,\tau)$, and is always close to any eigenfrequency ω_j of the structure. The shape of the chatter vibrations at the stability lobes can be characterized by $\hat{\mathbf{q}}(\omega_c)\mathbf{e}^{i\omega_c t}$, $\hat{\mathbf{r}}(P,\omega_c)\mathbf{e}^{i\omega_c t}$, and $\hat{h}(P,\omega_c)\mathbf{e}^{i\omega_c t}$ in modal, Cartesian, and normal coordinates, respectively.

The present approach describes an efficient method for the position-dependent identification of the stability lobes for cutting processes with flexible tool and flexible workpiece. The modal FRF matrix $\Phi_q(\omega)$ and the mode shapes $\mathbf{V}(P)$ of the structure can be calculated analytically via beam theory as described in Section 2 or numerically via FE methods. It is also possible to combine, for example, measurements for the FRF $\Phi_{t,r}(\omega)$ at the tool tip in Cartesian coordinates with numerical or analytical results for the workpiece dynamics. In this case, the FRF matrix $\Phi_r(P,\omega)$ of the combined structure in Cartesian coordinates can be determined by

$$\Phi_r(P,\omega)=\Phi_{t,r}(\omega)+\mathbf{V}_w(P)\Phi_{w,q}(\omega)\mathbf{V}_w^T(P), \tag{27}$$

with the $N_w \times N_w$ diagonal FRF matrix $\Phi_{w,q}(\omega)$ of the modal FRFs for the workpiece dynamics being similar to the definition in Eq. 18 with $j = 1,\dots N_w$. If the FRF matrix $\Phi_r(P,\omega)$ is known, the oriented transfer function $\sigma(P,\omega)$ can be determined via Eq. 23 and the stability lobes can be identified with Eqs. 24, 25, and 26.

The current approach offers several advantages which include (1) flexibility in using experimental, numerical, and analytical data to generate the combined FRF of the structure, and (2) the stability analysis is not restricted to a specific number of modes in one direction. This makes the described approach a significant generalization and an extension to prior works [7, 9, 13–16].

3.3 Stability evaluation via oriented transfer function

Applying Eq. 25 to 24 yields the relationship $\lambda_{\mathrm{R}}(P,\omega_{\mathrm{cr}},\tau) = -2\sigma_{\mathrm{R}}(P,\omega_{\mathrm{cr}})$ which is independent of the time delay τ. Using this relationship in Eq. 26 one obtains the well-known stability law of Tlusty [24] for the position-dependent oriented transfer function

$$b_{\mathrm{cr}}=-\frac{1}{2K_t\sigma_{\mathrm{R}}(P,\omega_{\mathrm{cr}})}. \tag{28}$$

Equation 28 reveals a relationship between the real part of the oriented transfer function and the critical limiting chip width b_{cr}, which holds for all spindle speeds Ω. In general, the position-dependent oriented transfer function $\sigma(P,\omega)$ is suitable for understanding the stability behavior of turning with flexible tool and flexible workpiece. In particular, the negative minimum of the real part $\sigma_{\mathrm{R}}(P,\omega_{\mathrm{cr}})$ of the oriented transfer function defines the minimum limiting chip width $min(b_{\mathrm{lim}})$. Thus, the real part of the oriented transfer function can be used for evaluating the system stability that depends on the variation of the structural or process parameters but is independent of a specific spindle speed Ω or cutting pressure K_t. This is useful for the optimization of machine tool development or process planning as demonstrated by the examples below.

4 Results

4.1 Machine tool model from the literature

In this subsection, a grooving process ($\psi_r = 90°$) based on parameters from the literature is studied [14]. In this example, a steel rod was turned. The normal direction is defined by $\mathbf{e}_n = (1,0,0)^T$, that is, only vibrations in x-direction affect the cutting force. The force in z-direction is zero ($k_r = 0$). The resulting oriented transfer function according to Eq. 23 is $\sigma = k_n\Phi_{xx} + \Phi_{xy}$. Consistent with Ref. [14] only a single mode for the tool dynamics parallel to the x-axis is considered. Thus, the y and z components of the mode shapes $\mathbf{v}_j$ are zero. The only non-zero component of the FRF matrix $\Phi_r(P,\omega)$ is $\Phi_{xx}(P,\omega)$, and the position-dependent oriented transfer function further simplifies to $\sigma(P,\omega) = k_n\Phi_{xx}(P,\omega)$. The parameters for the tool dynamics, the workpiece dynamics and the cutting force behavior are summarized in Table 1.

As mentioned above, the boundary conditions for the workpiece model are fixed at $\xi = 0$, and pinned or free at $\xi = L$, representing the turning process with or without tailstock, respectively. The x-component of the dominant mode shapes along the workpiece axis are shown in Fig. 2. The tool mode (green, thick) does not dependent on the axial coordinate ξ of the workpiece. For fixed-free boundary conditions (red, dashed), the highest workpiece flexibility appears at the free end of the workpiece. The eigenfrequency of the workpiece mode is 190.6 Hz. The mode shape

of the second bending mode with eigenfrequency 1195 Hz is not shown in Fig. 2. It has only a minor influence on the process dynamics due to its higher stiffness. For turning with tailstock, i.e., fixed-pinned boundary conditions, the highest workpiece flexibility can be found around $\xi = 0.3$ m as can be seen from the black (solid) curve in Fig. 2. Here, the eigenfrequency for the first bending mode is 836 Hz (see Table 1).

In Fig. 3, the dynamics of the cutting process at the cutting point $P = 0.3$ m is illustrated for the case with (black, solid) and without (red, dashed/thick) tailstock. Figure 3a depicts the real part $\sigma_R(P, \omega)$ of the oriented transfer function. According to Eq. 27, it is a superposition of the direct FRF of the tool and the workpiece. For both cases, the first peak around 100.6 Hz corresponds to the tool mode. The remaining peaks at 836 Hz for the tailstock-supported workpiece (black, solid), as well as the peaks at 190.6 and 1195 Hz for the fixed-free workpiece (red, dashed) correspond to the first bending modes of the workpiece. The amplitude of $\sigma_R(P, \omega)$ at the first workpiece mode is lower for turning with tailstock than for turning without tailstock. This is a direct consequence of the increased dynamic stiffness due to the tailstock support. As a result, the process is stabilized by the tailstock, which can be seen by an increased limiting chip width for a wide range of spindle speeds in Fig. 3b. The corresponding chatter frequencies ω_c are shown in Fig. 3c. It can be seen that in both cases for spindle speeds $\Omega \in [2150, 2350]$ rpm and $\Omega \in [3350, 3950]$ rpm, the stability is determined by the tool mode with chatter frequencies slightly larger than 100.6 Hz. Obviously, for these spindle speeds, the tailstock support does not stabilize the process (cf. Fig. 3b). In general, a stabilization of the process via a tailstock can be obtained only for spindle speeds with chatter frequencies around the workpiece eigenmodes.

In Fig. 4, the process dynamics are analyzed for fixed-free boundary conditions of the workpiece and a varying cutting point P. The solid (black) curves for $P = L = 0.5$ m correspond exactly to the cutting conditions from [14]. The stability lobes in Fig. 4b for this case coincide with the results from the literature. According to the shape of the dominant workpiece mode for fixed-free boundaries (see red, dashed curve in Fig. 2), the influence of the workpixece dynamics decreases for cutting points closer to the chuck, $P \to 0$. As a consequence, for decreasing P the amplitude of the oriented transfer function in Fig. 4a around the workpiece mode at 190.6 Hz decreases. Furthermore, as can be seen in Fig. 4b, the limiting chip width of the process increases for decreasing P. An exception can be seen for $P = 0.2$ m (green, thick). In this case, the global minimum of $\sigma_R(P, \omega)$ in Fig. 4a can be found around the tool mode at 100.6 Hz. However, according to Tlusty's law (28) the minimum of the real part $\sigma_R(P, \omega)$ of the oriented transfer function determines the limiting chip width. Thus, for spindle speeds $\Omega \in [2150, 2350]$ rpm and $\Omega \in [3350, 3950]$ rpm, no further stabilization of the process is possible by increasing the workpiece stiffness. Indeed, for $P = 0.2$ m the chatter frequencies, which are not shown here, are located around the eigenfrequency of the tool, whereas for $P = 0.4$ m and $P = 0.5$ m in the whole spindle speed interval $\Omega \in [2000, 6000]$ they are located around the workpiece eigenfrequency.

4.2 Mode interaction between tool and workpiece modes

Actually, the tool mode is slightly destabilized for an increasing workpiece stiffness. This can be seen in Fig. 3b and in Fig. 4b for spindle speeds $\Omega \in [2150, 2350]$ rpm and $\Omega \in [3350, 3950]$ rpm, where the chatter frequency is close to the eigenfrequency of the tool. Although the shape, stiffness, or damping of the tool mode does not change with changing boundary conditions of the workpiece or varying cutting position, there is a mode interaction between the tool and the workpiece mode due to the regenerative effect. Mathematically, this can be explained by a decreasing real part $\sigma_R(P, \omega)$ of the oriented transfer function around the tool eigenmode at 100.6 Hz for decreasing influence of the workpiece dynamics in Fig. 4a. Since the negative minimum of $\sigma_R(P, \omega)$ determines the stability, the limiting chip width corresponding to the tool eigenmode decreases with increasing workpiece stiffness. In general, all eigenmodes with eigenfrequencies smaller (larger) than the workpiece

Table 1 Process parameters for the examples in Section 4

Workpiece parameters				
$\rho = 7600$ kg/m^3	$E = 180 \times 10^9$ N/m^2	$L = 0.5$ m	$D = 0.07$ m	$I = 1.18 \times 10^{-6}$ m^4
Modal parameters	mass kg	damping ζ	frequency Hz	mode shape
Dominant tool mode	50.0	0.032	100.6	$\mathbf{v}_{t,1} = (1, 0, 0)^T$
Workpiece 1st mode (fixed-free):	14.6	0.025	190.6	$\mathbf{v}_{w,1}(0.5\text{ m}) = (\ \ 1.99, 0, 0)^T$
Workpiece 2nd mode (fixed-free):	14.6	0.025	1195.0	$\mathbf{v}_{w,2}(0.5\text{ m}) = (-1.99, 0, 0)^T$
Workpiece 1st mode (fixed-pinned):	14.6	0.025	836.0	$\mathbf{v}_{w,1}(0.3\text{ m}) = (1.51, 0, 0)^T$
Cutting force coefficients	$K_t = 2000 \times 10^6$ N/m^2	$k_n = 0.342$	$k_r = 0$	

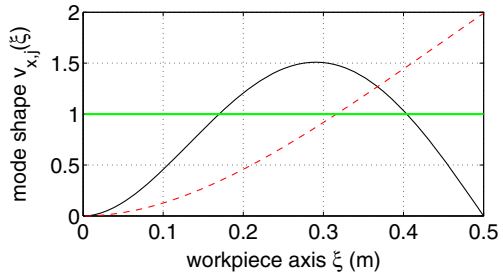

Fig. 2 Mode shapes in x-direction for the dominant tool mode (*green, thick*), as well as the dominant workpiece mode with fixed-free (*red, dashed*) and fixed-pinned (*black, solid*) boundaries. The mode shape of the tool does not change along the workpiece axis

eigenmode are stabilized (destabilized) by increasing the workpiece flexibility.

The physical explanation of the mode interaction is as follows. First, a rigid workpiece and a flexible tool where no mode interaction is possible are considered. For an unstable process, a tool tip vibration $\mathbf{r}_t(t)$ with a chatter frequency ω_c slightly larger than the eigenfrequency of the tool occurs. The energy introduced by the regenerative effect is larger than the dissipation due to damping [25]. If a flexible workpiece is considered, vibrations of the workpiece $\mathbf{r}_w(P,t)$ with the same chatter frequency ω_c occur. For workpiece eigenfrequencies larger than the chatter frequency ω_c, the energy balance of the regenerative effect of the workpiece vibration is negative. In other words, energy is not only dissipated by tool damping but also by workpiece damping and the self-excitation of the workpiece due to the regenerative effect. If the workpiece flexibility is increased, more energy is dissipated by the regenerative effect at the workpiece. As a result, an instability of the tool eigenmode can be stabilized by increasing the flexibility of workpiece or other eigenmodes with higher eigenfrequencies.

4.3 Realistic machine tool model

In this subsection, a complex realistic model for the tool dynamics is considered, where experimental data for the FRFs at the tool tip are used. Cylindrical turning at the cutting point $P = L = 0.5$ m without tailstock (fixed-free boundaries) is considered. The force has components along x, y, and z. The normal direction is defined by $\mathbf{e}_n^T = (\sin\psi_r, 0, \cos\psi_r)$. Thus, depending on the lead angle ψ_r, vibrations in the xz-plane can become unstable, whereas vibrations in y-direction are forced vibrations. The cutting force coefficients and the parameters for the steel rod are taken from the example from the literature (see Table 1), except for a larger workpiece diameter $D = 0.12$ m. The mode shape of the dominant bending mode of the workpiece is similar to the red (dashed) curve in Fig. 2. However, due to the increased diameter of the workpiece, the workpiece

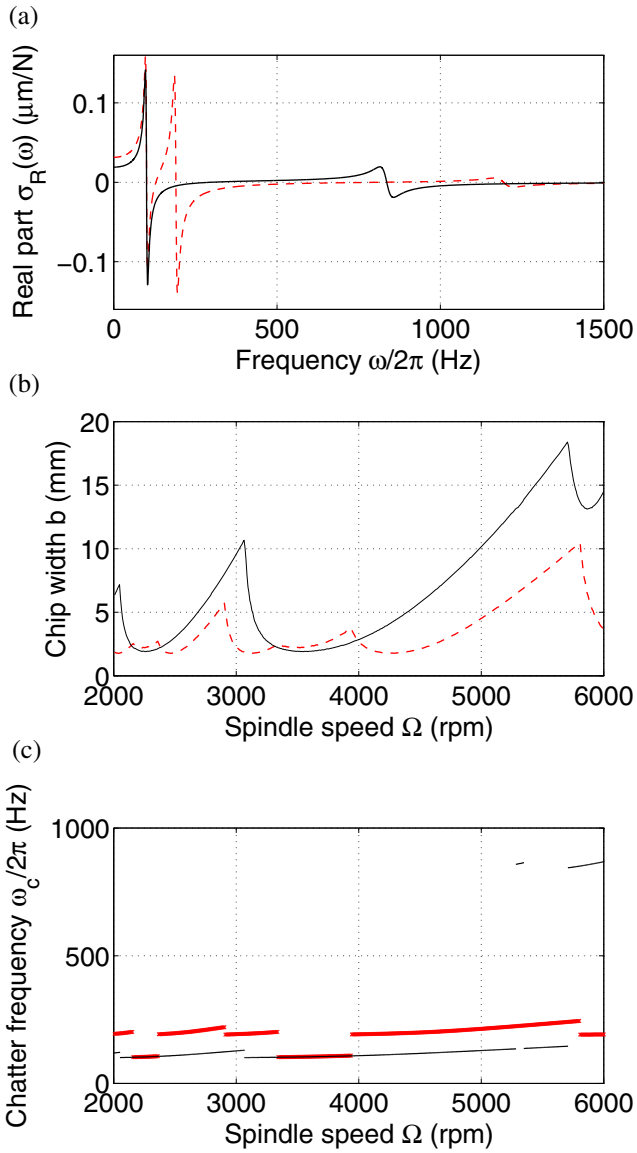

Fig. 3 **a** Real part $\sigma_R(P,\omega)$ of the oriented transfer functions, **b** stability lobes, and **c** chatter frequencies are shown for grooving with (*black, solid*) and without (*red, dashed/thick*) tailstock. Tailstock support increases the dynamic stiffness of the workpiece modes, and workpiece instabilities can be suppressed

stiffness and eigenfrequeny are increased. Figure 5 shows the magnitude of the relevant FRFs at the tool tip of a CNC lathe Gildemeister CTX 400 E. The direct and cross FRFs at the tool tip of a lathe were obtained by impact hammer tests. The dynamic behavior for vibrations in the x- and z-directions is shown in Figs. 5a, b. The dynamic behavior at the tool tip is dominated by a low-frequency mode of the machine tool structure around 140 Hz and a high-frequency tool mode slightly below 1600 Hz. The maximum magnitude of the FRFs can be found at the tool mode around 1600 Hz for excitation and response in the z-direction. In contrast to the simplified model in the example above, the

cross FRFs cannot be neglected for an accurate characterization of the dynamics at the tool tip of a real lathe. To elaborate, the directions of the vectors $\mathbf{v}_{t,j}$ for the mode shapes at the tool tip in Cartesian coordinates are not perpendicular to the x, y, or z directions. The workpiece is assumed to be rigid in the z-direction and the direct FRF in the x-direction is shown in Fig. 5c. The eigenfrequency of the first bending mode for the workpiece with diameter $d = 0.12$ is 326 Hz. The oriented transfer function according to Eq. 23 can be specified by

$$\begin{aligned}\sigma = s\left((\Phi_{t,xx}+\Phi_{w,xx})k_n s+\Phi_{t,xy}+\Phi_{t,xz}k_n c\right)\\ +c\left(\Phi_{t,zx}k_n s+\Phi_{t,zy}+\Phi_{t,zz}k_n c\right),\end{aligned} \tag{29}$$

where $s = \sin\psi_r$ and $c = \cos\psi_r$.

In Fig. 6, the stability lobes and the corresponding chatter frequencies are shown for varying lead angle ψ_r. For comparison of the stability behavior, the stability lobes are presented in terms of the depth of cut $a_r = b\cos\psi_r$ rather than pure chip width b. Theoretically, for zero lead angle $\psi_r = 0$, the workpiece dynamics $\Phi_{w,xx}$ have no influence on the oriented transfer function $\sigma = \Phi_{t,zy} + \Phi_{t,zz}k_n$ and the stability lobes. For increasing lead angle, the influence of the vibrations in the x-direction on the chip chip thickness

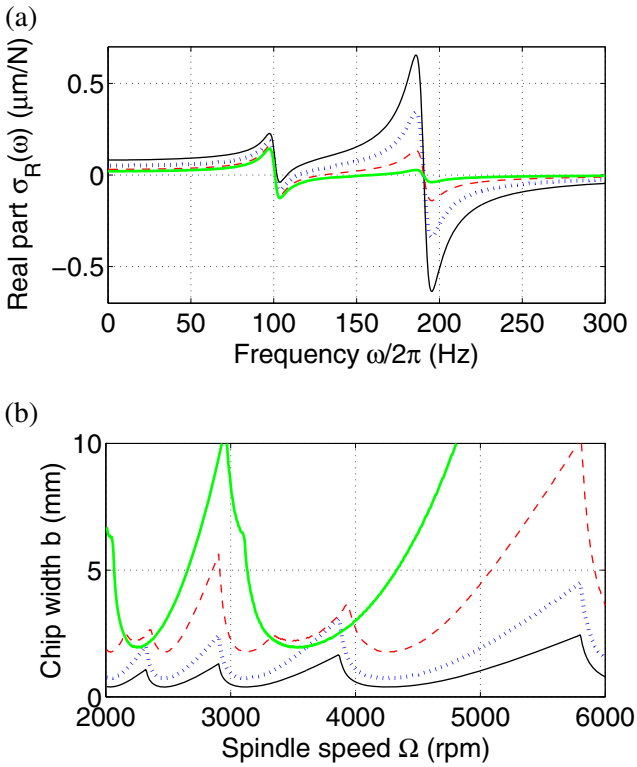

Fig. 4 The workpiece flexibility decreases for cutting points P closer to the chuck. **a** For decreasing P, the peak of the real part $\sigma_R(P,\omega)$ of the oriented transfer functions around the workpiece mode decreases. **b** The process is stabilized for smaller P ($P = 0.5m$: *black,solid*; $P = 0.4m$: *blue*, *dotted*; $P = 0.3m$: *red, dashed*; $P = 0.2m$: *green, thick*)

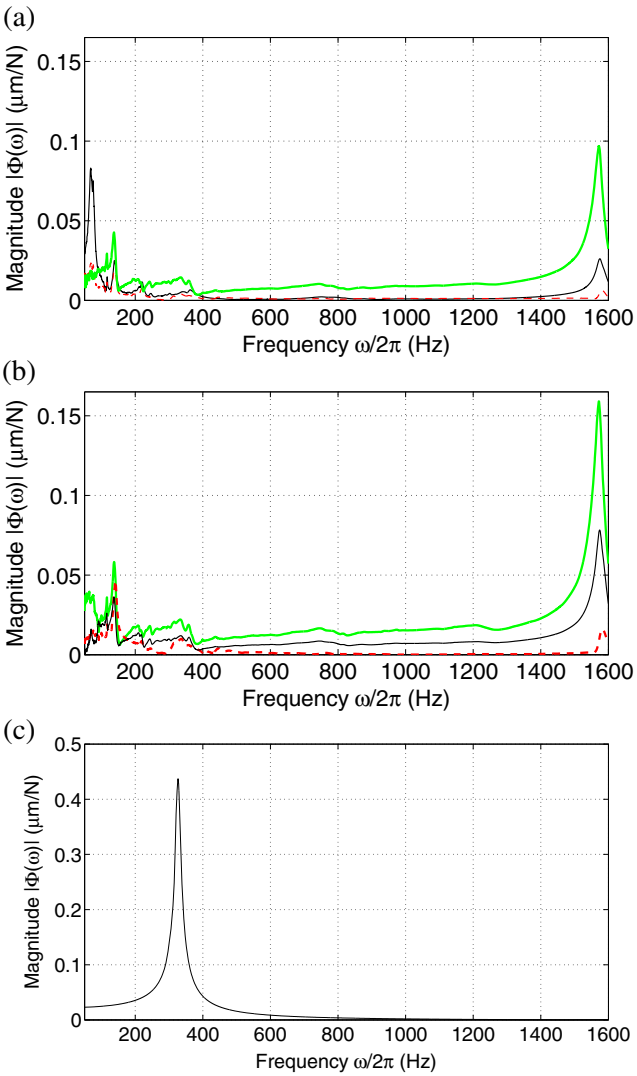

Fig. 5 Magnitude of measured tool FRFs for vibrations in x (**a**) and z (**b**) direction in response to a force in x (*black, solid*), y (*red, dashed*) and z (*green, thick*) direction, and magnitude of the analytically determined direct workpiece FRF $\Phi_{w,xx}(P,\omega)$ in x-direction (**c**) with $P = L$, $D = 0.12m$ and fixed-free boundaries

increases. In Fig. 6a, the stability lobes for $\psi_r = 15°$ (black, solid) are composed of slender lobes corresponding to the tool mode and wide lobes corresponding to the structural mode of the machine tool. The associated chatter frequencies in Fig. 6b are around 1600 and 140 Hz, respectively. No instability of the workpiece eigenmode occurs. For the larger lead angle $\psi_r = 30°$ (red, dashed), the flexibility of the workpiece in x-direction becomes more important. Consequently, e.g., for spindle speeds $\Omega \in [3450, 3650]$ rpm and $\Omega \in [4050, 4350]$ rpm, new lobes associated to the first bending mode of the workpiece appear. The corresponding chatter frequencies are slightly larger than the eigenfrequency of the workpiece mode at 326 Hz as can be seen in Fig. 6b. The slender lobes for the tool mode with

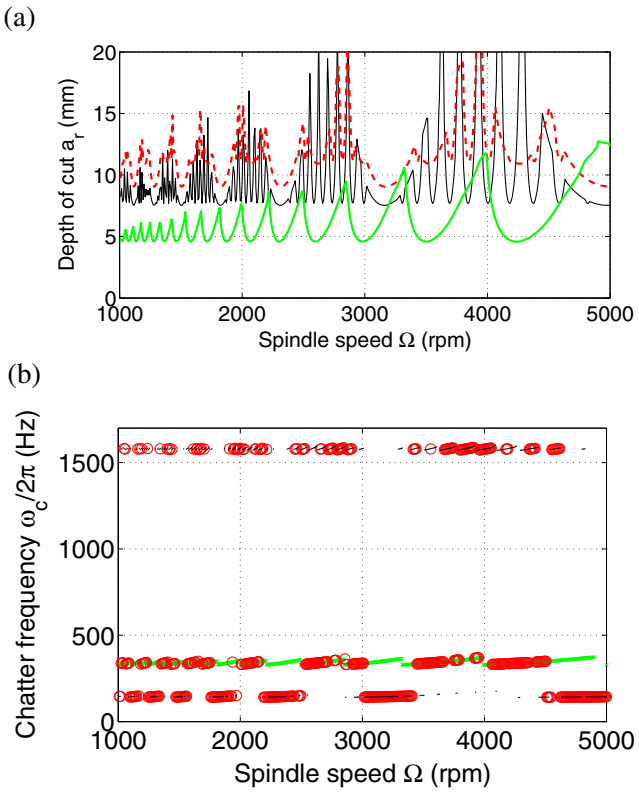

Fig. 6 Stability lobes (**a**) and chatter frequencies (**b**) for cylindrical turning without tailstock and varying lead angles $\psi_r = 15°$ (*black, solid*), $\psi_r = 30°$ (*red, dashed/circles*), and $\psi_r = 45°$ (*green, thick*). An optimal lead angle can be found around $\psi_r = 30°$, where tool and workpiece instabilities are balanced

high chatter frequencies are stabilized. This is due to the fact that the excitation of the tool mode is lower because for larger lead angle ψ_r the excitation in z-direction decreases. Furthermore, in contrast to $\psi_r = 15°$, for $\psi_r = 30°$, the wide structural modes with low chatter frequencies are also stabilized. A reason for this can be the effect of mode interaction as explained in detail in Section 4.2. For a lead angle $\psi_r = 45°$ (green, thick), the excitation of the workpiece mode in x-direction is further increased. The stability lobes are almost everywhere associated with an instability of the workpiece mode. As a result, the maximum limiting depth of cut can be obtained for a lead angle around $\psi_r = 30°$, where tool and workpiece instabilities are balanced. The presented efficient investigation of the nontrivial effect of the lead angle on the stability of the process can be useful for process planning.

5 Conclusion

A universal model for analyzing the dynamics of turning a flexible workpiece with a compliant tool at varying cutting points has been presented. The model can be used to combine analytical, numerical, and experimental data for the tool and the workpiece dynamics and is not restricted to the consideration of a specific number of modes or a specific spatial direction. The stability lobes can be identified via a frequency domain method similar to [23], which is very efficient even for a large number of modes. The real part $\sigma_R(P, \omega)$ of the oriented transfer function is used to study the effect of process parameters on the stability of the cutting process.

In particular, the effect of the flexible workpiece on the stability lobes has been analyzed for two examples based on experimental data and results from the literature. The qualitative and quantitative changes in the stability behavior were shown for varying cutting point, lead angle, and boundary conditions, i.e., turning with and without tailstock. The main observations can be summarized as follows.

1. An increasing influence of the workpiece dynamics due to a change of the cutting point, lead angle, or boundary condition, obviously, leads to a destabilization of the workpiece modes.
2. Counterintuitively, increasing the stiffness of the workpiece can destabilize tool modes with eigenfrequencies lower than the first workpiece eigenfrequency due to the interaction between tool and workpiece modes via the cutting process.

The results reveal potential strategies for increasing quality and productivity of metal cutting if both the tool and the workpiece are flexible. One interesting effect is the stabilization of low-frequency modes at the tool tip by decreasing the dynamic stiffness of the workpiece. The main disadvantage may be a destabilization of workpiece modes at higher frequencies. However, these high-frequency vibrations are typically suppressed by process damping [26].

Moreover, the presented position-dependent oriented transfer function approach can be combined with the recent results in [23] to study the stability in milling of flexible workpieces.

References

1. Zhao MX, Balachandran B (2001) Dynamics and stability of milling process. Int J Solids Struct 38(10–13):2233–2248
2. Khasawneh FA, Mann B, Insperger T, Stépán G (2009) Increased stability of low-speed turning through a distributed force and continuous delay model. J Comput Nonlin Dyn 4(4):041,003
3. Butcher E, Bobrenkov O, Bueler E, Nindujarla P (2009) Analysis of milling stability by the Chebyshev collocation method: Algorithm and optimal stable immersion levels. J Comp Nonlin Dyn 4(3):031,003
4. Otto A, Radons G (2013) Application of spindle speed variation for chatter suppression in turning. CIRP J Manuf Sci Technol 6(2):102–109

5. Yu SD, Shah V (2009) Theoretical and experimental studies of chatter in turning for uniform and stepped workpieces. J Vibr Acoustics 130(6):061,005
6. Gang L (2009) Study on deformation of titanium thin-walled part in milling process. J Mater Proc Technol 209(6):2788–2793
7. Han X, Ouyang H, Wang M, Hassan N, Mao Y (2012) Self-excited vibration of workpieces in a turning process. Proc Inst Mech Eng C J Mech Eng Sci 226(8):1958–1970
8. Song Q, Ai X, Tang W (2011) Prediction of simultaneous dynamic stability limit of time-variable parameters system in thin-walled workpiece high-speed milling processes. Int J Adv Manuf Technol 55(9–12):883–889
9. Urbikain G, de Lacalle LL, Campa F, Fernandez A, Elias A (2012) Stability prediction in straight turning of a flexible workpiece by collocation method. Int J Mach Tools Manuf 54–55:73–81
10. Eksioglu C, Kilic Z, Altintas Y (2012) Discrete-time prediction of chatter stability, cutting forces, and surface location errors in flexible milling systems. J Manuf Sci Engin 134(6):061,006
11. Thevenot V, Arnaud L, Dessein G, Cazenave-Larroche G (2006) Integration of dynamic behaviour variations in the stability lobes method: 3d lobes construction and application to thin-walled structure milling. Int J Adv Manuf Technol 27(7–8):638–644
12. Bravo U, Altuzarra O, de Lacalle LL, Sanchez J, Campa F (2005) Stability limits of milling considering the flexibility of the workpiece and the machine. Int J Mach Tools Manuf 45(15):1669–1680
13. Chen C, Tsao Y (2006) A stability analysis of turning a tailstock supported flexible work-piece. Int J Mach Tools Manuf 46(1):18–25
14. Vela-Martinez L, Jauregui-Correa J, Rubio-Cerda E, Herrera-Ruiz G, Lozano-Guzman A (2008) Analysis of compliance between the cutting tool and the workpiece on the stability of a turning process. Int J Mach Tools and Manuf 48(9):1054–1062
15. Sekar M, Srinivas J, Kotaiah K, Yang S (2009) Stability analysis of turning process with tailstock-supported workpiece. Int J Adv Manuf Technol 43(9–10):862–871
16. Chen D, Lin B, Han Z, Zhang Y (2013) Study on the optimization of cutting parameters in turning thin-walled circular cylindrical shell based upon cutting stability. Int J Adv Manuf Technol 69 (1–4):891–899
17. Altintas Y (2000) Manufacturing automation: metal cutting mechanics, machine tool vibrations, and CNC design. Cambridge University Press, New York
18. Otto A, Radons G (2015) Stability analysis of machine-tool vibrations in the frequency domain. Proc 12th IFAC TDS Workshop, Ann Arbor
19. Pakdemirli M, Boyaci H (2002) Effect of non-ideal boundary conditions on the vibrations of continuous systems. J Sound Vibr 249(4):815–823
20. Zatarain M, Bediaga I, Muñoa J, Insperger T (2010) Analysis of directional factors in milling: importance of multi-frequency calculation and of the inclusion of the effect of the helix angle. Int J Adv Manuf Techn 47:535–542
21. Adhikari S (2006) Damping modelling using generalized proportional damping. J Sound Vibr 293(1–2):156–170
22. Budak E, Ozlu E (2007) Analytical modeling of chatter stability in turning and boring operations: A multi-dimensional approach. CIRP Annals 56:401–404
23. Otto A, Rauh S, Kolouch M, Radons G (2014) Extension of tlusty's law for the identification of chatter stability lobes in multi-dimensional cutting processes. Int J Mach Tools Manuf 82–83:50–58
24. Danek O, Polacek M, Spacek J, Tlusty J (1962) Selbsterregte Schwingungen an Werkzeugmaschinen. VEB Technik, Berlin
25. Al-Regib E, Ni J, Lee SH (2003) Programming spindle speed variation for machine tool chatter suppression. Int J Mach Tools Manuf 43(12):1229–1240
26. Tyler C, Schmitz T (2013) Analytical process damping stability prediction. J Manuf Proc 15(1):69–76